Facile Synthetic Route for Surface-Functionalized Magnetic Nanoparticles: Cell Labeling and Magnetic Resonance Imaging Studies

Hyun Jung Chung,[†,#] Haeshin Lee,[‡,§,#] Ki Hyun Bae,[†] Yuhan Lee,[†] Jongnam Park,[⊥] Seung-Woo Cho,[∥] Jin Young Hwang,[△] Hyunwook Park,[△] Robert Langer,[▽,○,□] Daniel Anderson,[▽,○,□,*] and Tae Gwan Park[†,§,*]

[†]Department of Biological Sciences, [‡]Department of Chemistry, [§]The Graduate School of Nanoscience & Technology, Korea Advanced Institute of Science and Technology (KAIST), Daejeon, 305-701, Republic of Korea, [⊥]Energy Engineering, Ulsan National Institute of Science and Technology, Ulsan, Republic of Korea 689-805, [∥]Department of Biotechnology, Yonsei University, Seoul, 120-749, Republic of Korea, [△]Department of Electrical Engineering, KAIST, Daejeon, 305-701, Republic of Korea, [▽]David H. Koch Institute for Integrative Cancer Research, Massachusetts Institute of Technology, Cambridge, Massachusetts 02139, United States, [○]Department of Chemical Engineering, Massachusetts Institute of Technology, Cambridge, Massachusetts 02139, United States, and [□]Harvard—Massachusetts Institute of Technology Division of Health Sciences and Technology, Cambridge, Massachusetts 02139, United States . [#]These authors contributed equally to this work.

ABSTRACT Currently available methods to stably disperse iron oxide nanoparticles (IONPs) in aqueous solution need to be improved due to potential aggregation, reduction of superparamagnetism, and the use of toxic reagents. Herein, we present a facile strategy for aqueous transfer and dispersion of organic-synthesized IONPs using only polyethylene glycol (PEG), a biocompatible polymer. A library of PEG derivatives was screened, and it was determined that amine-functionalized six-armed PEG, 6(PEG-NH_2), was the most effective dispersion agent. The 6(PEG-NH_2)-modified IONPs (IONP-6PEG) were stable after extensive washing, exhibited high superparamagnetism, and could be used as a platform material for secondary surface functionalization with bioactive polymers. IONP-6PEG biofunctionalized with hyaluronic acid (IONP-6PEG-HA) was shown to specifically label mesenchymal stem cells and demonstrate MR contrast potential with high r_2 relaxivity (442.7 $s^{-1}mM^{-1}$) compared to the commercially available Feridex (182.1 $s^{-1}mM^{-1}$).

KEYWORDS: iron oxide nanoparticles · dispersion · PEG · surface functionalization · MRI

Magnetic nanoparticles are of interest in biomedical imaging because of their unique physical and chemical properties.[1] In particular, superparamagnetic iron oxide nanoparticles (IONPs), a negative contrast agent in MR imaging, have been utilized for various biomedical applications, such as cancer imaging, cellular labeling, and magnetofection.[2−5] IONPs have been routinely synthesized by precipitation of iron salts in aqueous solution.[6,7] Recently, thermal decomposition in organic solvents has been reported to produce monodisperse IONPs with precise control of superparamagnetism and size relative to those prepared from aqueous phase synthesis.[2,4,8,9]

In order to utilize monodisperse, organic-synthesized IONPs for biomedical imaging, they must be capable of stable dispersion in aqueous media.[2−4] Numerous descriptions of phase transfer and stabilization of IONPs have been reported.[4,10−14] Examples include the formation of core—shell nanoparticles with a thick shell layer of cross-linked dextran[10] or silica[11] and coating with surfactants [cetyl trimethylammonium bromide (CTAB), citrate, *etc.*][4] and poly(ethylene glycol) (PEG)-based polymers including PEG-fatty acid,[12] PEG-phospholipid,[13] and poly(ethylene oxide)-poly(propylene oxide-)-poly(ethylene oxide) (PEO-PPO-PEO) triblock copolymer (Pluronic).[14] However, significant challenges remain for these solutions, including nonbiodegradability and reduced superparamagnetism due to the thick shell or partially hydrophobic layer,[10,11] use of toxic reagents,[4,10] colloidal aggregations,[3,4] and difficulty in the removal of polymeric micelles.[12−14]

In this study, we developed a facile route to produce well-dispersed IONPs in aqueous solution with high stability and biocompatibility, using an amine-functionalized, star-shaped PEG derivative, followed by functionalization with bioactive polymer for cellular imaging (Figure 1). We hypothesized that PEGs with small end-functional groups could bind to the surface of IONPs and provide a thin, stable monolayer coating around them.[15−17] The high hydrophilicity of PEG chains would render the particles

* Address correspondence to tgpark@kaist.ac.kr, dgander@mit.edu.

Received for review October 6, 2010 and accepted May 28, 2011.

Published online May 28, 2011
10.1021/nn201198f

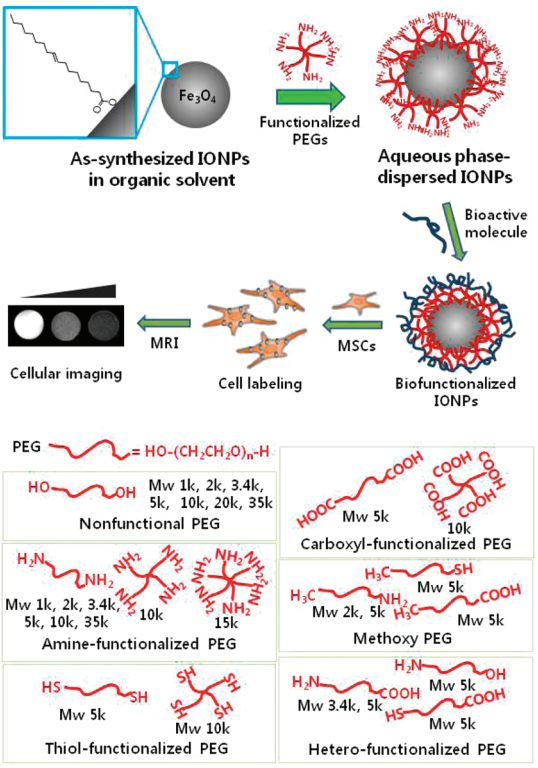

Figure 1. Schematic illustration of the procedure for dispersion of IONPs in an aqueous phase using a library of PEG derivatives followed by functionalization with bioactive molecules for cellular labeling and imaging. Inset shows oleic acid on IONP surface.

soluble and stabilized in the aqueous media. Herein, we demonstrated that six-arm amine-functionalized PEG (6(PEG-NH_2)) is a superior dispersion agent for the monodisperse IONPs, allowing successful IONP transfer and stabilization without the need of any additional reagents or incorporation of hydrophobic domains. IONPs modified by 6(PEG-NH_2) (IONP-6PEG) have a thin PEG layer on the surface, show no apparent aggregation, and retain their original superparamagnetism. These particles are then amenable to bioconjugation, due to the presence of surface-exposed amine groups in 6(PEG-NH_2). Hyaluronic acid modified IONP-6PEGs were used to label mesenchymal stem cells for MR imaging and cellular trafficking.

RESULTS AND DISCUSSION

Monodisperse and superparamagnetic IONPs (10 nm in size) coated with oleic acid and dispersed in chloroform were prepared.[8] For the transfer of the IONPs from an organic to an aqueous phase, a library of PEG derivatives was evaluated for potential utility as surface-modifying agents, with the goal of identifying structures that could facilitate effective transfer without the need of any additional chemical modification reactions. The PEG library included PEG derivatives with variations in structural configurations (linear, four-arm, and six-arm), molecular weights (1, 2, 3.4, 5, 10, 15 kDa, *etc.*), and small functional groups on the PEG end-groups (−NH_2, −SH, −OH, −CH_3, *etc.*) (Table S1). The PEG and the IONPs were co-dissolved in chloroform, dried under vacuum, and added with distilled water.[15] The first visual indication of successful aqueous phase transfer of the IONPs was the apparent formation of a dispersion solution with a clear brown color. Several of the commercial PEG derivatives, including −NH_2-, −COOH-, and −SH-functionalized PEGs and native diol PEGs (HO-PEG-OH) with molecular weight greater than 20 kDa, exhibited successful phase transfer of IONPs (Figure 1). After the phase transfer, the unbound PEG molecules dissolved in the IONP dispersion were removed by extensive washing, and the stability of the IONPs was examined by UV absorption measurement at 350 nm (Figure 2A). Absorption at 350 nm is known as a characteristic peak of IONPs, which has been widely used for their quantitative characterization.[18,19] Substantial absorbance was measured for well-dispersed IONPs in an aqueous medium, but the poorly dispersed IONPs were aggregated and then precipitated, resulting in a clear supernatant. After washing, only the amine-functionalized PEGs with M_w larger than 5 kDa resulted in a stable dispersion. With increasing values of the M_w, the number of branched chains, and the number of functionalities, higher absorbance values could be attained. This indicates more efficient transfer and dispersion. Above all, six-arm amine-functionalized PEG (6(PEG-NH_2)) showed the highest absorbance and efficient transfer. Size measurements by dynamic light scattering showed that the IONPs dispersed with 6(PEG-NH_2) resulted in the smallest hydrodynamic diameter (28.2 ± 7.4 nm), compared to ones stabilized by four-arm amine-functionalized PEG (4(PEG-NH_2), 40.8 ± 8.5 nm) or amine-bifunctionalized PEG (H_2N-PEG-NH_2, 36.9 ± 12.4 nm), possibly due to the tighter, multivalent binding (Figure 2B). Zeta potential values showed that the IONPs stabilized by the amine bifunctional and multifunctional PEGs exhibited overall positive surface charges (2.5 ± 1 to 12.8 ± 2.7 mV), while ones dispersed with a methoxy-PEG with a monofunctional amine group (mPEG-NH_2) were close to neutral (0.4 ± 2.6 mV) (Figure 2C). This evidenced the binding of amine groups to the IONP surface, with some portion of them projecting outward. The slight decrease in the zeta potential value of IONPs dispersed with 6(PEG-NH_2) compared to that of 4(PEG-NH_2) can be due to the denser shielding effect.[20] According to these results, IONPs dispersed with 6(PEG-NH_2) (IONP-6PEG) showed the most successful transfer and stabilization and were further characterized. Thermogravimetric analysis (TGA) showed that the amount of PEG on the IONP-6PEGs was about 25.2 w/w % of the total particle weight, as determined from the significant mass change at 381.7 °C due to decomposition of PEG (Figure S1A). A minor change observed at 253.6 °C represented oleic acid, which constituted 6.9 w/w %

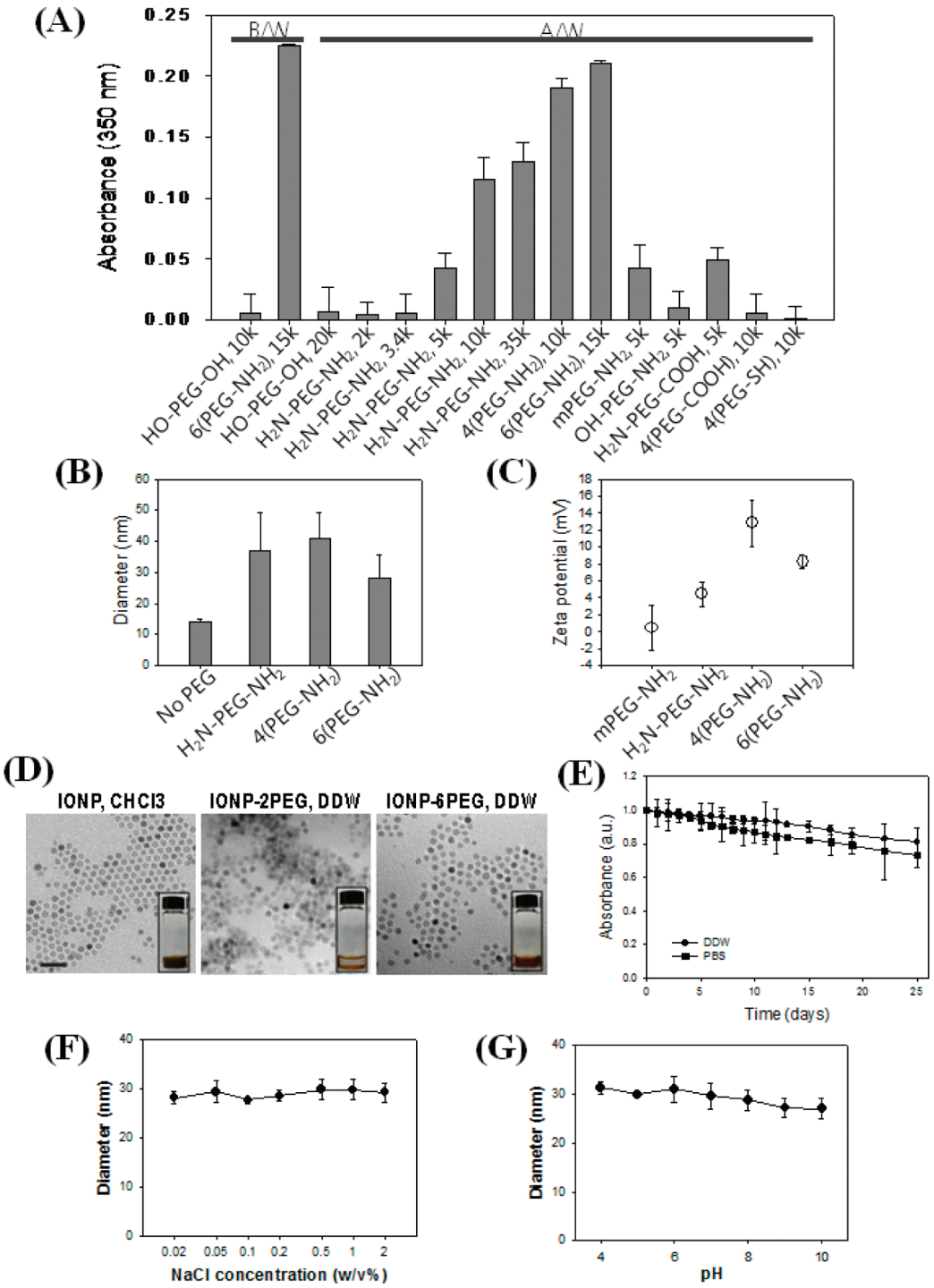

Figure 2. Phase transfer and stabilization of IONPs. (A) Evaluation of dispersed IONPs using a library of commercial PEG derivatives measured by UV absorbance at 350 nm (B/W: before washing, A/W: after washing). (B) DLS measurements and (C) zeta potential values of IONPs stabilized with amine-functionalized PEGs (H_2N-PEG-NH_2, M_w 10 000; 4(PEG-NH_2), M_w 10 000; and 6(PEG-NH_2), M_w 15 000). (D) TEM of IONPs stabilized (DDW) with 6(PEG-NH_2) (IONP-6PEG) and H_2N-PEG-NH_2 (M_w 5000) (IONP-2PEG), or in chloroform before transfer (IONP, $CHCl_3$) (size bar: 50 nm). Insets show photographs of the IONP dispersions. (E) Long-term colloidal stability of IONP-6PEGs by measuring absorbance at 350 nm. DLS measurements for determining stability of IONP-6PEGs in various (F) salt concentrations and (G) pHs.

of the whole particle. Differential scanning calorimetry (DSC) showed that IONP-6PEGs exhibited a large endothermic peak at 41.8 °C due to the crystallization of PEG (Figure S1B). The slight decrease in temperature (~9 °C) compared to the typical melting peak of PEG (50.9 °C) suggested that multiple amine groups of 6(PEG-NH_2) were possibly intercalated by interacting with carboxylic acid groups in oleic acids.[14] The IONP-6PEGs were also observed by TEM, which showed that IONP-6PEGs were well dispersed in the form of individual

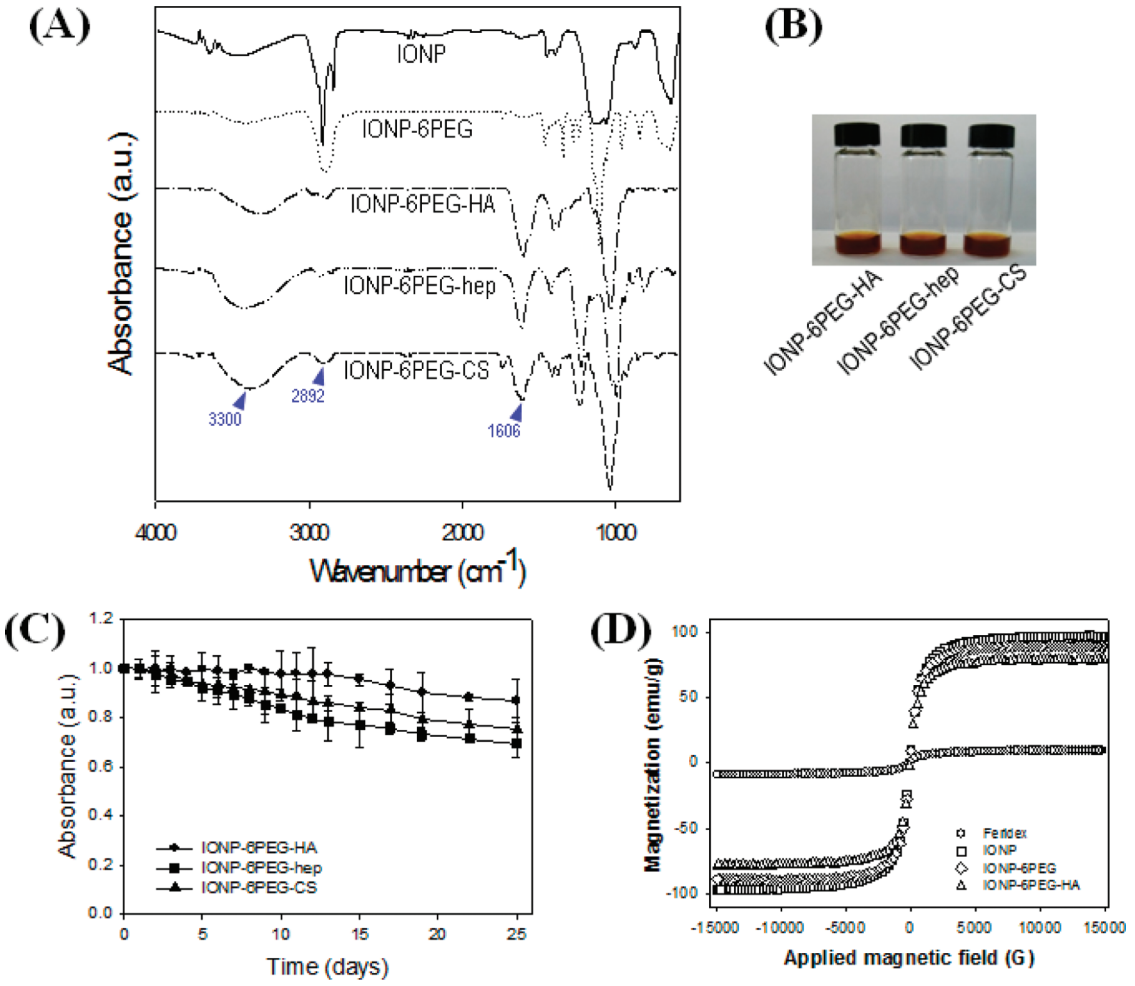

Figure 3. Characterization of the biofunctionalized IONPs. (A) FT-IR spectra and (B) gross views of IONP-6PEGs after biofunctionalization. (C) Long-term stability of biofunctionalized IONPs by absorbance measurements at 350 nm. (D) Magnetic properties of IONPs measured by VSM.

particles, in contrast to the IONPs dispersed with NH_2-PEG-NH_2, which were agglomerated (Figure 2D). The long-term stability of IONP-6PEGs in aqueous media was examined by monitoring the absorbance values at 350 nm. Figure 2E shows that ~90% of the total particles were well-dispersed in water for 25 days. It is well known that IONPs usually become unstable and easily aggregate in high salt conditions. The IONP-6PEGs showed significantly high stability in phosphate-buffered saline (PBS) solution, with over 80% of the particles stably dispersed for at least 20 days. DLS measurements in various salt concentrations and pHs also confirmed the high stability of IONP-6PEGs. Figure 2F,G show that IONP-6PEGs retained hydrodynamic diameters of 27−31 nm and existed as individual particles, even in high salt concentrations up to 2 w/v % and extreme pHs (pH 4 or 10). The above results all showed that 6(PEG-NH_2) was immobilized on the IONP surface by the binding of amine groups, forming a thin polymeric coating layer. This allowed transfer and stable dispersion of the IONPs, while providing surface functionalities for further modification.

The strong binding of the amine-functionalized PEGs might be due to direct Fe-nitrogen coordination on the IONP surface[16,17,21] and/or ionic interactions between the carboxyl groups of oleic acids and amine groups of PEGs.[14]

With high colloidal stability and surface functionalities, the IONP-6PEGs could be chemically modified with various bioactive molecules. Biofunctional polymers such as hyaluronic acid (HA), heparin (hep), and chondroitin sulfate (CS) could be easily conjugated onto the surface of the IONP-6PEGs (IONP-6PEG-HA, IONP-6PEG-hep, and IONP-6PEG-CS). The carboxyl groups on the polysaccharides were reacted with the surface-exposed amine groups on the IONP-6PEGs by EDC/NHS chemistry. The presence of immobilized polysaccharides on the IONP-6PEGs was confirmed by Fourier transform infrared spectroscopy (Figure 3A). The peaks around 2892 and 1606 cm^{-1} refer to hydroxyl and carbonyl groups, which are abundant in the polysaccharides, demonstrating successful bioconjugation. Attempts to immobilize HA, heparin, and chondroitin sulfate in the absence of coupling reagents, EDC

and NHS, resulted in unsuccessful surface immobilizations. Furthermore, the polysaccharides were not immobilized onto the surface of IONPs that were dispersed by linear mPEG-NH_2, which would be due to the lack of surface-exposed amine groups. These results indicate that the polysaccharide immobilization occurs *via* formation of amide bonds by the coupling agents. The biofunctionalized IONP-6PEGs retained their appearance as a stable, dark brown colloid with no sign of aggregation or precipitation (Figure 3B). The hydrodynamic sizes were increased for the biofunctionalized IONP-6PEGs, ranging from 79 to 203 nm, probably due to (1) the presence of an additional layer of the high M_w polymer and/or (2) some extent of interparticle cross-linking (Figure S2A). The DLS sizes of IONP-6PEGs after polysaccharide functionalization were increased to ~75 nm for IONP-6PEG-HA, whereas the IONPs functionalized by heparin and chondroitin sulfate showed 150−200 nm sizes. This increase in size might be due to cluster formation of IONPs by chemical cross-linking between the particles. The polydispersity index of the sizes was also larger for functionalized IONP-6PEGs than before functionalization (~0.15) and even more for IONP-6PEG-hep (~0.39) and IONP-6PEG-CS (~0.31) compared to IONP-6PEG-HA (~0.2). The surface charges of the biofunctionalized IONP-6PEGs were slightly negative, ranging from -9.1 ± 1.5 to -3.1 ± 1.9 mV, further confirming the immobilization of the anionic polysaccharides on the surfaces (Figure S2B). The long-term stability of the biofunctionalized IONP-6PEGs was also examined (Figure 3C). All functionalized particles showed high stability in aqueous buffer solution, with 70−90% of the particles remaining well dispersed up to 25 days.

The magnetic properties of biofunctionalized IONP-6PEGs were investigated using a vibrating sample magnetometer (VSM). Figure 3D shows that IONP-6PEG and IONP-6PEG-HA exhibited little changes in superparamagnetic magnetization compared to as-synthesized IONPs. The saturated magnetization (M_s) values of IONP-6PEG and IONP-6PEG-HA were 89.4, and 79.0 emu/g, which were significantly higher than that of Feridex (Bayer HealthCare Pharmaceuticals), a commercial formulation of iron oxide nanoparticles (9.5 emu/g). These results revealed that the phase-transfer process and bioconjugation reaction produced aqueous IONPs with high superparamagnetism. According to previous reports, a coating layer comprising a completely hydrophilic polymer would be greatly advantageous compared to amphiphilic coatings, due to easy access of water protons to the particle surfaces, resulting in superior proton relaxivity.[16]

HA has been widely utilized for fabrication or modification of biomedical materials due to their wide interactions and functions on cells and tissues in the biological environment.[22,23] In this study, we utilized HA as a functional moiety for targeted labeling of human mesenchymal stem cells (MSCs). The labeling efficiency of IONP-6PEG-HA on MSCs was investigated by confocal imaging and iron content quantification. It has been well known that most primary cells, such as endothelial cells, smooth muscle cells, and MSCs, exhibit extremely low uptake efficiency of small-particle materials.[24] Figure S3A shows that IONP-6PEG-HA could efficiently label the MSCs, as can be seen by the green fluorescence within the cell interior. It has been reported that MSCs abundantly express CD44.[25] The amount of cellular uptake was much higher for IONP-6PEG-HA (145.9 ± 15.2 ng Fe/10^5 cells) than IONP-6PEG (63 ± 12.3 ng Fe/10^5 cells), showing that the presence of HA on the surface greatly enhanced internalization of the particles (Figure S3B). When an excess of HA was added to the cells prior to IONP-6PEG-HA, the extent of cellular uptake was significantly decreased (53.8 ± 5.1 ng Fe/10^5 cells), showing that the free HA molecules prevented direct interactions between IONP-6PEG-HA and cell surfaces. This result suggests that the labeling of MSCs with IONP-HA might be due to CD44-mediated endocytosis. Feridex showed considerably lower cellular uptake (45.1 ± 3.9 ng Fe/10^5 cells) compared to IONP-6PEG-HA. HCT116 and HeLa cells, which are known to express high and normal levels of CD44, respectively, were also treated with IONP-6PEG-HA and observed by confocal microscopy. HCT116 cells showed much higher uptake levels, while HeLa cells showed moderate levels of uptake, giving further evidence for the specific interactions between IONP-6PEG-HAs and MSCs (Figure S4). The viability of MSCs treated with IONP-6PEG-HA was also assessed, which showed that over 95% of the MSCs treated at concentrations up to 50 μg Fe/mL were viable (Figure S3C,D). Treatment of IONP coated with CTAB as the control caused severe cytotoxicity due to the quaternary ammonium moiety of CTAB.[26] These results show that IONP-6PEG-HA could efficiently and safely label the MSCs by a cell-specific receptor-mediated process. However, to unambiguously prove the CD44-mediated endocytosis process, further in-depth studies should be carried out.

Finally, the MSCs labeled with IONP-6PEG-HA were subjected to MR imaging using a 3.0 T MRI system. *In vitro* MRI of the MSCs labeled with IONP-6PEG-HA showed greatly enhanced negative T_2 contrast, whereas the labeled MSCs in the presence of excess HA showed marginal enhancement due to the lower cellular uptake (Figure 4A). The T_2 relaxation times for the cells treated with 1 μg/mL IONP-6PEG-HA, 2 μg/mL IONP-6PEG-HA, and 2 μg/mL IONP-6PEG-HA in the presence of excess HA, and Feridex were 57.8, 156.3, 277.8, and 454.5 ms, respectively. Assuming there were no changes in the r_2 relaxivity during each step of

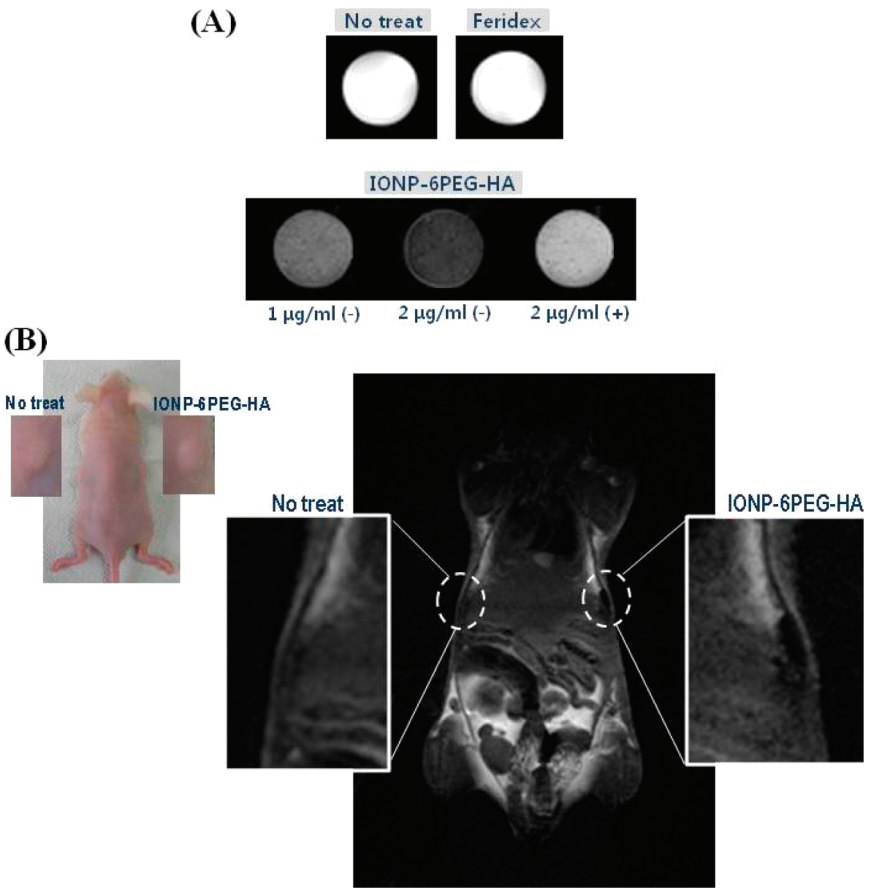

Figure 4. MR imaging of MSCs labeled with IONP-6PEG-HA: (A) T_2-weighted images of labeled MSCs by treating with Feridex (2 μg/mL Fe) or IONP-6PEG-HA (1 or 2 μg/mL Fe) in the absence (−) or presence (+) of excess HA, or MSCs without any treatment (No treat). (B) *In vivo* MR imaging by subcutaneous injection of nontreated MSCs or MSCs treated with IONP-6PEG-HA (n = 3).

surface modification, the values of the particles were obtained from normalization by the amount of particle uptake. The r_2 relaxivity was 442.7 s^{-1} mM^{-1} for IONP-6PEG-HA, which is significantly higher than that of Feridex (182.1 s^{-1} mM^{-1}) and comparable to the reported values.[11,27] In fact, however, it is expected that the r_2 relaxivity value of IONP-6PEG-HA would be slightly lower than IONP-6PEG, due to the surface-bound polymers preventing access of water molecules to the IONP surface.[28,29] Finally, the IONP-6PEG-HA-labeled MSCs were subjected to MR imaging *in vivo* in a mouse model. The unlabeled MSCs were barely detected, whereas the IONP-6PEG-HA-labeled MSCs were clearly detected as dark spots in the subcutaneous region (Figure 4B). Labeling of therapeutic cells with magnetic nanoparticles and their subsequent administration *in vivo* can be advantageous in allowing trafficking of the cells and the curing processes by live imaging.[25,30] Previous studies have reported difficulty in performing these tasks due to either low labeling efficiency for MRI detection or high toxicity of the magnetic material. Therefore, IONP-6PEG-HA, exhibiting high labeling efficiency, low cytotoxicity, and superior MRI contrast for MSCs, holds great promise as a labeling tool for cell therapeutics. Further in-depth studies on evaluation of cell viability after *in vivo* injection should be carried out for applications in *in vivo* tracking of therapeutic cells.

CONCLUSIONS

Herein, we developed a facile route for aqueous-phase dispersion and biofunctionalization of monodisperse IONPs. A simple polymeric coating method allowed an easy organic-to-aqueous phase transfer of monodisperse IONPs. By screening a commercial library of PEG derivatives, 6(PEG-NH_2) was shown to provide the most efficient transfer and stabilization of the IONPs. The current formulation method using 6(PEG-NH_2) as a dispersion agent for IONPs was meritorious in producing well-dispersed IONPs with high colloidal stability, good superparamagnetism, and surface functionalities for further modifications. The aqueous-dispersed IONPs using 6(PEG-NH_2) (IONP-6PEG) were conjugated with various bioactive molecules on the surface. IONP-6PEGs biofunctionalized with HA (IONP-6PEG-HA) was used as a labeling probe for human mesenchymal stem cells. IONP-6PEG-HA could

efficiently label the MSCs with low toxicity and showed greatly enhanced MRI contrast *in vitro* as well as *in vivo*. We expect that the IONP stabilized by 6(PEG-NH_2) can be widely utilized for practical applications as an imaging probe for various purposes in biomedical diagnosis.

MATERIALS AND METHODS

Materials. Superparamagnetic Fe_3O_4 nanoparticles were synthesized by a previous method.[8] The synthetic procedure involved formation of an iron-oleate complex, which produces IONPs with an oleic acid coating on the surface of the IONPs. The library of PEG derivatives was obtained from Laysan Bio, Inc. (Arab, AL).

Instrumental Analyses. UV absorption of the IONPs was measured using Nanodrop (ND-1000, Thermo Scientific, Wilmington, DE). Dynamic light scattering (DLS) and zeta potential measurements were performed using ZetaPlus (Malvern Instruments, Worcestershire, UK). Transmission electron microscopy (TEM) was performed using a Philips CM20. Thermogravimetric analysis was performed using a TG209F3 (Netzcsh, Germany), and differential scanning calorimetry was done using a DSC204F1 (Netzsch, Germany). Fourier transform infrared spectroscopy (FT-IR) was performed using an IFS66 V/S (Bruker Optiks, Germany).

Phase Transfer and Aqueous Dispersion of IONPs. A library of various end-functionalized PEGs was screened and examined as transfer agents for IONPs from organic to aqueous phase. In brief, 500 μL of 2 w/v % PEG in chloroform was added with 500 μL of 2 mg/mL IONPs in chloroform and dried under vacuum. For water dispersion, 500 μL of deionized distilled water (DDW) was added and inverted several times for thorough dispersion. If the dispersion appeared as a transparent, brown-colored solution with no sign of insoluble aggregates or precipitates, it was determined to be successfully transferred, and otherwise, not transferred. For purification of the surface-coated IONPs by removal of free PEGs in solution, the IONPs were extensively washed in DDW using centrifugal filters with a molecular weight cutoff (MWCO) of 100 000 (Amicon Ultra, Millipore) and/or dialysis (MWCO 1 000 000, SpectraPor, Spectrum Laboratories).

Biofunctionalization of Aqueous-Dispersed IONPs. Aqueous-dispersed IONPs were biofunctionalized by reacting with bioactive anionic polysaccharides. Briefly, 500 mg of hyaluronic acid (17 kDa, Lifecore Biomedical), heparin (12 kDa, Wako Chemical Industries), and chondroitin sulfate (Sigma-Aldrich) were dissolved in DDW and freeze-dried. For reaction with IONPs, 200 mg of hyaluronic acid, heparin, or chondriotin sulfate (500 μmol) was dissolved in 5 mL of DDW and added with 1.9 mg of 1-ethyl-3-[3-dimethylaminopropyl]carbodiimide hydrochloride (EDC) (50 μmol) and 2.4 mg of *N*-hydroxysuccinimide (NHS) (100 μmol). Then, 500 μL of 6(PEG-NH_2)-coated and purified IONPs (5 mg) in DDW was slowly added to the reaction solution with magnetic stirring. For observing intracellular uptake by confocal microscopy, HA labeled with fluorescein was used for reaction instead of HA. Fluorescein-labeled HA was prepared by reacting 500 mg of HA (1 mmol) with 19.2 mg of EDC (0.1 mmol), 23 mg of NHS (0.1 mmol), and 3.5 mg of 5-aminofluorescein (0.01 mmol), followed by extensive dialysis (MWCO 5000) and freeze-drying. After 12 h, the reacted IONPs were extensively washed with DDW using Amicon filters (MWCO 100 000).

Cellular Labeling Using Biofunctionalized IONPs. Bone marrow-derived human mesenchymal stem cells, HCT116, and HeLa cells were cultured in minimum essential medium-α (α-MEM), RPMI 1640, and Dulbecco's modified essential medium (DMEM), respectively, all supplemented with 10 v/v % fetal bovine serum (FBS), 100 U/mL penicillin, and 100 μg/mL streptomycin. All reagents for cell culture were purchased from Gibco (Gaithersburg, MD). Each of the cells was seeded onto microscopic culture slides or T75 culture flasks. Twelve hours before treating with IONPs, the cells were preincubated in serum-free media or 1 w/v % solution of HA in serum-free media. Then IONPs were added to the cells at a final concentration of 2 μg/mL for 12 h. For microscopic observations, the treated cells were washed three times with phosphate-buffered saline solution. For observing live and dead cells by confocal microscopy, cells were added to a solution of 2 μM calcein AM and 4 μM ethidium homodimer (Invitrogen, Carlsbad, CA) and incubated for 30 min. To observe internalization of fluorescently labeled IONPs into cells, the cells were fixed in 4 w/v % paraformaldehyde solution and mounted with Vectashield containing 4′,6-diamidino-2-phenylindole (Vector Laboratories, Burlingame, CA) for confocal microscopy (LSM710, Carl Zeiss, Jena, Germany). To quantitatively assess cellular uptake, treated cells were trypsinized and washed, and iron content was measured either by inductively coupled plasma atomic emission spectrometry (ICP-AES) or by Prussian blue staining and UV−visible spectrometry. For ICP-AES, cells were freeze-dried, treated with nitric acid, and diluted with DDW. For Prussian blue staining, cells were treated with 750 μL of 2 v/v % hydrochloride solution for 30 min and then with 250 μL of 2 w/v % potassium ferrocyanide solution for 15 min, and the absorbance at 711 nm was measured using a spectrophotometer (Nanodrop). The amount of cellular uptake was calculated on the basis of a standard curve obtained with IONP dispersions. Cell viability was also quantitatively measured using the cell counting kit-8 (CCK-8, Dojindo Laboratories, Kumamoto, Japan). To cells treated with IONPs was added a 0.1 volume of CCK-8 solution, the solution was incubated for 2 h, and the optical density at 450 nm was measured using a microplate reader (model 550, Biorad, Hercules, CA). The percentage of viable cells (%) was calculated on the basis of calibration from a standard curve for fresh, nontreated cells.

MR Imaging. MSCs labeled with the biofunctionalized IONPs were observed *in vitro* and *in vivo* using a 3.0 T MRI system (ISOL Tech., Korea) equipped with a customized quadrature radio-frequency coil of 9 cm diameter. For imaging *in vitro*, the labeled MSCs were fixed in gel phantoms made of 1 w/v % agarose, and the T_2-weighted images were obtained by a spin−echo pulse sequence with the following parameters: TR/TE = 3000/100 ms, FOV = 100 × 100 mm^2, matrix = 128 × 128, flip angle = 90°, average number = 2, voxel size = 0.78 × 0.78 × 2 mm^3. T_2 relaxation times of the labeled MSCs were obtained by calculation from a series of images using the same parameters but varying the TE value from 15 to 300 ms. r_2 relaxivity was calculated by normalization of T_2 relaxation times with concentrations of IONPs obtained from the amount of particle uptake and binding on cells, assuming that the density of Fe_3O_4 nanoparticles was 5 g/cm^3.[31] For *in vivo* MR imaging, the labeled MSCs (2×10^5, 100 μL) were injected subcutaneously into the dorsal side of nude mice, and after 1 day the T_2-weighted images were obtained by a fast spin−echo sequence using the following parameters: TR/TE = 3000/100 ms, FOV = 100 × 100 mm^2, matrix = 256 × 256, slice thickness = 2 mm, average number = 4, voxel size = 0.39 × 0.39 × 3 mm^3. For both *in vitro* and *in vivo* MRI, three images were obtained for each sample and analyzed.

Acknowledgment. This study was financially supported by the National Research Foundation (NRF, South Korea): Development of Medical Technology Program (2010-0028765; H.L.), World Class University Program (R31-2008-000-10071-0; H.L.), and Korea Biotech R&D Program (2010K001356; H.L.). We also thank Alnylam and Controlled Release of Macromolecules (EB000244; D.G.A.).

Supporting Information Available: Table of commercial PEG library, TGA and DSC data, additional DLS and zeta potential measurements, confocal images of other labeled cell lines. This material is available free of charge *via* the Internet at http://pubs.acs.org.

REFERENCES AND NOTES

1. Cai, W.; Chen, X. Nanoplatforms for Targeted Molecular Imaging in Living Subjects. *Small* **2007**, *3*, 1840–1854.
2. Gupta, A. K.; Gupta, M. Synthesis and Surface Engineering of Iron Oxide Nanoparticles for Biomedical Applications. *Biomaterials* **2005**, *26*, 3995–4021.
3. McCarthy, J. R.; Weissleder, R. Multifunctional Magnetic Nanoparticles for Targeted Imaging and Therapy. *Adv. Drug Delivery Rev.* **2008**, *60*, 1241–1251.
4. Laurent, S.; Forge, D.; Port, M.; Roch, A.; Robic, C.; Vander Elst, L.; Muller, R. N. Magnetic Iron Oxide Nanoparticles: Synthesis, Stabilization, Vectorization, Physicochemical Characterizations, and Biological Applications. *Chem. Rev.* **2008**, *108*, 2064–2110.
5. Sosnovik, D. E.; Weissleder, R. Emerging Concepts in Molecular MRI. *Curr. Opin. Biotechnol.* **2007**, *18*, 4–10.
6. Petri-Fink, A.; Chastellain, M.; Juillerat-Jeanneret, L.; Ferrari, A.; Hofmann, H. Development of Functionalized Superparamagnetic Iron Oxide Nanoparticles for Interaction with Human Cancer Cells. *Biomaterials* **2005**, *26*, 2685–2694.
7. Matuszewski, L.; Persigehl, T.; Wall, A.; Schwindt, W.; Tombach, B.; Fobker, M.; Poremba, C.; Ebert, W.; Heindel, W.; Bremer, C. Cell Tagging with Clinically Approved Iron Oxides: Feasibility and Effect of Lipofection, Particle Size, and Surface Coating on Labeling Efficiency. *Radiology* **2005**, *235*, 155–161.
8. Park, J.; An, K.; Hwang, Y.; Park, J. G.; Noh, H. J.; Kim, J. Y.; Park, J. H.; Hwang, N. M.; Hyeon, T. Ultra-Large-Scale Syntheses of Monodisperse Nanocrystals. *Nat. Mater.* **2004**, *3*, 891–895.
9. Park, J.; Lee, E.; Hwang, N. M.; Kang, M.; Kim, S. C.; Hwang, Y.; Park, J. G.; Noh, H. J.; Kim, J. Y.; Park; *et al.* One-Nanometer-Scale Size-Controlled Synthesis of Monodisperse Magnetic Iron Oxide Nanoparticles. *Angew. Chem., Int. Ed.* **2005**, *44*, 2872–2877.
10. Kircher, M. F.; Mahmood, U.; King, R. S.; Weissleder, R.; Josephson, L. A Multimodal Nanoparticle for Preoperative Magnetic Resonance Imaging and Intraoperative Optical Brain Tumor Delineation. *Cancer Res.* **2003**, *63*, 8122–8125.
11. Lu, C. W.; Hung, Y.; Hsiao, J. K.; Yao, M.; Chung, T. H.; Lin, Y. S.; Wu, S. H.; Hsu, S. C.; Liu, H. M.; Mou; *et al.* Bifunctional Magnetic Silica Nanoparticles for Highly Efficient Human Stem Cell Labeling. *Nano Lett.* **2007**, *7*, 149–154.
12. Yang, J.; Lee, T.; Lee, J.; Lim, E.; Hyung, W.; Lee, C.; Song, Y. J.; Suh, J.; Yoon, H.; Huh; *et al.* Synthesis of Ultrasensitive Magnetic Resonance Contrast Agents for Cancer Imaging Using PEG-Fatty Acid. *Chem. Mater.* **2007**, *19*, 3870–3876.
13. Nitin, N.; LaConte, L. E. W.; Zurkiya, O.; Hu, X.; Bao, G. Functionalization and Peptide-Based Delivery of Magnetic Nanoparticles as an Intracellular MRI Contrast Agent. *J. Biol. Inorg. Chem.* **2004**, *9*, 706–712.
14. Qin, J.; Laurent, S.; Jo, Y. S.; Roch, A.; Mikhaylova, M.; Bhujwalla, Z. M.; Muller, R. N.; Muhammed, M. A High-Performance Magnetic Resonance Imaging T2 Contrast Agent. *Adv. Mater.* **2007**, *19*, 1874–1878.
15. Portet, D.; Denizot, B.; Rump, E.; Lejeune, J. J.; Jallet, P. Nonpolymeric Coatings of Iron Oxide Colloids for Biological Use as Magnetic Resonance Imaging Contrast Agents. *J. Colloid Interface Sci.* **2001**, *238*, 37–42.
16. Duan, H.; Kuang, M.; Wang, X.; Wang, Y. A.; Mao, H.; Nie, S Reexamining the Effects of Particle Size and Surface Chemistry on the Magnetic Properties of Iron Oxide Nanocrystals: New Insights into Spin Disorder and Proton Relaxivity. *J. Phys. Chem.* **2008**, *112*, 8127–8131.
17. Zhang, H.; Lee, M.; Hogg, M. G.; Dordick, J. S.; Sharfstein, S. T. Gene Delivery in Three-Dimensional Cell Cultures by Superparamagnetic Nanoparticles. *ACS Nano* **2010**, *4*, 4733–4743.
18. Kim, M.; Chen, Y.; Liu, Y.; Peng, X. Super-Stable, High-Quality Fe_3O_4 Dendron-Nanocrystals Dispersible in Both Organic and Aqueous Solutions. *Adv. Mater.* **2005**, *17*, 1429–1432.
19. Mamedov, A.; Ostrander, J.; Aliev, F.; Kotov, N. A. Stratified Assemblies of Magnetite Nanoparticles and Montmorillonite Prepared by the Layer-by-Layer Assembly. *Langmuir* **2000**, *16*, 3941–3949.
20. Mok, H.; Bae, K. H.; Ahn, C.; Park, T. G. PEGylated and MMP-2 Specifically DePEGylated Quantum Dots: Comparative Evaluation of Cellular Uptake. *Langmuir* **2009**, *25*, 1645–1650.
21. Salazar-Salinas, K.; Jauregui, L. A.; Kubli-Garfias, C.; Seminario, J. M. Molecular Biosensor Based on a Coordinated Iron Complex. *J. Chem. Phys.* **2009**, *130*, 105–101.
22. Morra, M. Engineering of Biomaterials Surfaces by Hyaluronan. *Biomacromolecules* **2005**, *6*, 1205–1223.
23. Lee, Y.; Lee, H.; Kim, Y. B.; Kim, J.; Hyeon, T.; Park, H.; Messersmith, P. B.; Park, T. G. Bioinspired Surface Immobilization of Hyaluronic Acid on Monodisperse Magnetite Nanocrystals for Targeted Cancer Imaging. *Adv. Mater.* **2008**, *20*, 4154–4157.
24. Bulte, J. W.; Douglas, T.; Witwer, B.; Zhang, S. C.; Strable, E.; Lewis, B. K.; Zywicke, H.; Miller, B.; van Gelderen, P.; Moskowitz; *et al.* Magnetodendrimers Allow Endosomal Magnetic Labeling and In Vivo Tracking of Stem Cells. *Nat. Biotechnol.* **2001**, *19*, 1141–1147.
25. Sackstein, R.; Merzaban, J. S.; Cain, D. W.; Dagia, N. M.; Spencer, J. A.; Lin, C. P.; Wohlgemuth, R. Ex Vivo Glycan Engineering of CD44 Programs Human Multipotent Mesenchymal Stromal Cell Trafficking to Bone. *Nat. Med.* **2008**, *14*, 181–187.
26. Tarantola, M.; Schneider, D.; Sunnick, E.; Adam, H.; Pierrat, S.; Rosman, C.; Breus, V.; Sonnichsen, C.; Basche, T.; Wegener, J.; *et al.* Cytotoxicity of Metal and Semiconductor Nanoparticles Indicated by Cellular Micromotility. *ACS Nano* **2009**, *3*, 213–222.
27. Lee, J.; Huh, Y.; Jun, Y.; Seo, J.; Jang, J.; Song, H.; Kim, S.; Cho, E.; Yoon, H.; Suh, J.; *et al.* Artificially Engineered Magnetic Nanoparticles for Ultra-Sensitive Molecular Imaging. *Nat. Med.* **2007**, *13*, 95–99.
28. LaConte, L. E. W.; Nitin, N.; Zurkiya, O.; Caruntu, D.; O'Connor, C. J.; Hu, X.; Bao, G. Coating Thickness of Magnetic Iron Oxide Nanoparticles Affects R_2 Relaxivity. *J. Magn. Reson. Imaging* **2007**, *26*, 1634–1641.
29. Duan, H.; Kuang, M.; Wang, X.; Wang, Y. A.; Mao, H.; Nie, S. Reexamining the Effects of Particle Size and Surface Chemistry on the Magnetic Properties of Iron Oxide Nanocrystals: New Insights into Spin Disorder and Proton Relaxivity. *J. Phys. Chem.* **2008**, *112*, 8127–8131.
30. Kraitchman, D. L.; Heldman, A. W.; Atalar, E.; Amado, L. C.; Martin, B. J.; Pittenger, M. F.; Hare, J. M.; Bulte, J. W. M. In Vivo Magnetic Resonance Imaging of Mesenchymal Stem Cells in Myocardial Infarction. *Circulation* **2003**, *107*, 2290–2293.
31. Bae, K. H.; Kim, Y. B.; Lee, Y.; Hwang, J. Y.; Park, H. W.; Park, T. G. Bio-inspired Synthesis and Characterization of Gadolinium-Labeled Magnetite Nanoparticles for Dual Contrast T1- and T2-weighted Magnetic Resonance Imaging. *Bioconjugate Chem.* **2010**, *21*, 505–512.